Long-range proximity effect in aluminum thin films with regions of nearly identical transition temperatures

Y. K. Kwong,* K. Lin,† M. Park, M. S. Isaacson, and J. M. Parpia
School of Applied and Engineering Physics and Laboratory of Atomic and Solid State Physics, Cornell University, Ithaca, New York 14853
(Received 11 September 1991)

We have investigated the resistive transition of dirty aluminum thin films whose transition temperature is spatially modulated by $\sim 2-4\%$ along the current path. At current densities as high as 600 A/cm^2, the system exhibits a single homogeneous transition for modulation lengths up to 50 μm, an order of magnitude longer than predicted by current theories. In the limit that the modulation length is $<50\ \mu$m, the T_c depends sensitively and monotonically on the ratio of the lengths of the etched and the unetched regions (d_1/d_2), but only weakly on their absolute magnitudes. This behavior is reproduced for T_c modulation parallel or perpendicular to the current flow. For samples with a controlled aperiodic (Fibonacci) modulation, the T_c is compatible with that of periodically modulated films. The dependence of the T_c on d_1/d_2 can be fitted to a simple Ginzburg-Landau theory which assumes that the effective pair coherence length is long in comparison with the modulation period. Despite the good fit, data for the full range of experimentally accessible modulation length scales are not consistent with a more detailed microscopic theory. We believe this long-range proximity effect is not the consequence of pair tunneling, but is a manifestation of the long distance over which quasiparticle phase coherence is maintained in a two-dimensional metal film.

I. INTRODUCTION

We have examined the anomalously long-range superconducting proximity effect in a two-dimensional (2D) analog of a modulated-T_c superlattice. This system was prepared by surface-damaging selected regions of an otherwise uniform aluminium thin film. The technique permits us to study the proximity effect in the limit that the T_c's in a "two-component" system are similar, while simultaneously constraining other transport properties of the higher- and lower-T_c regions to be approximately the same. This is an unexplored regime since previous experiments[1,2] on the proximity effect typically utilize two distinct metals, which would, in general, entail rather different T_c's and associated transport properties.

The accepted theory for describing the proximity effect at dirty superconducting-normal (S-N) interfaces is due to de Gennes[2,3] and Werthamer[4] (dGW). Numerous experiments were carried out, chiefly in the 1960s, and agreement between experiment and theory was shown to be good.[1,2] Subsequent theoretical[5] and experimental[6,7] work was carried out to encompass clean systems. In keeping with standard terminology, the "N" region may be a superconductor above its T_c.

In both the dirty- and clean-limit theories, the superconducting order parameter decays exponentially on the N side of a S-N interface with a characteristic range, called K_N^{-1}. In the dGW description of a dirty system, for $T_{cS} > T \gg T_{cN}$, K_N^{-1} is equal to the so-called normal coherence length, $(\hbar D/2\pi k_B T)^{1/2}$. Here, D is the quasiparticle diffusion constant, and T_{cN} is the T_c of the N region. As T approaches T_{cN} from above, K_N^{-1} diverges,[1] to leading order in the reduced temperature as $[(n(T/T_{cN})]^{-1/2}$. Even at $T/T_{cN} \sim 1.01$, K_N^{-1} is not expected to exceed $\sim 1\ \mu$m in dirty aluminum thin films when $D \sim 50$ cm^2/s. For S-N-S systems with the N region substantially longer than 1 μm, the critical current density J_c should be vanishingly small since J_c is proportional to $\exp(-K_N d_N)$, where d_N is the length of the N region. Yet, we have found[8,9] that the observed proximity effect in our modulated-T_c structures is substantially more robust, and is quantitatively incompatible with the dGW theory. Despite the apparent inconsistency, it is unclear why our dirty-limit system should be outside the regime of validity of this theory.

In this paper, we will first describe the fabrication techniques used to prepare these modulated-T_c structures. In particular, the reactive-ion etching process used to locally suppress the T_c of the aluminum film by a few percent will be discussed. We will present the resistive transitions of these modulated structures, emphasizing first the long length scale ($>50\ \mu$m) and large critical current density (>600 A/cm^2) exhibited by the proximity effect. We then focus on the limit when the modulation period is sufficiently small ($<50\ \mu$m) so that the modulated structures exhibit single sharp resistive transitions. Effects of modulation direction and quasiperiodic modulation will be described. Data in the single-transition limit can be compared with different theoretical models, making precise the anomalous nature of this system. In conclusion, we will suggest a possible mechanism which may be responsible for the anomalously long range of the observed proximity effect.

II. THE SAMPLES

An aluminum thin film is first prepared by thermal evaporation and a lift-off process on a photolithographically patterned Si_3N_4/Si substrate. The nominal film thickness used throughout this study is 250 Å, while the typical width and length are 200 μm and 2 mm, respectively. The typical diffusion constant D of the films is $\sim 50\,cm^2/s$, as determined from the temperature dependence of the upper critical field close to T_c.[10] This value of D corresponds to a mean free path l of ~ 100 Å. Since l is substantially smaller than the intrinsic clean-limit coherence length of aluminium ($\sim 1.3\,\mu$m), our films are always in the dirty limit as far as the properties in the superconducting state are concerned.

The substrate on which the aluminum film has been deposited is then coated with resist material. Photolithography is, once again, performed to expose selected regions along the film, with the remaining (undeveloped) resist acting as the etch mask in subsequent processing steps. The sample is then subjected to a plasma of CHF_3 and O_2 gases. This process has the effect of suppressing the T_c by ~ 2–$4\,\%$, without appreciably affecting other transport properties. (The details of the fabrication and etching process are reported elsewhere.[11])

Photolithography permits any arbitrary configurations of lower-T_c (etched) and higher-T_c (unetched) regions to be defined on an otherwise continuous film. Two possible configurations pertinent to this work are shown schematically in Fig. 1, in which the T_c is modulated periodically in a direction perpendicular [Fig. 1(a)] and parallel [Fig. 1(b)] to the current flow. For nomenclature purposes, we define the T_c's of the etched and unetched section as T_{c1} and T_{c2}, respectively. The length of the etched and unetched section along the direction of T_c modulation is d_1 and d_2, respectively. The period of modulation d_1+d_2 is Λ, and the T_c difference $T_{c2}-T_{c1}$ is ΔT_c.

Figure 2 is a schematic layout of a typical (4 mm)^2 sample. Each sample typically contains sixteen films together with associated current and voltage leads suitable for four-point resistance measurements in a ^{3}He cryostat. This permits films with different configurations of d_1 and d_2 (e.g., d_1/d_2 is varied while d_1 is fixed) to be prepared simultaneously on a single substrate under identical conditions. On each sample, a uniformly etched and a uniformly unetched film are always available for control. Their T_c's operationally define T_{c1} and T_{c2}, respectively.

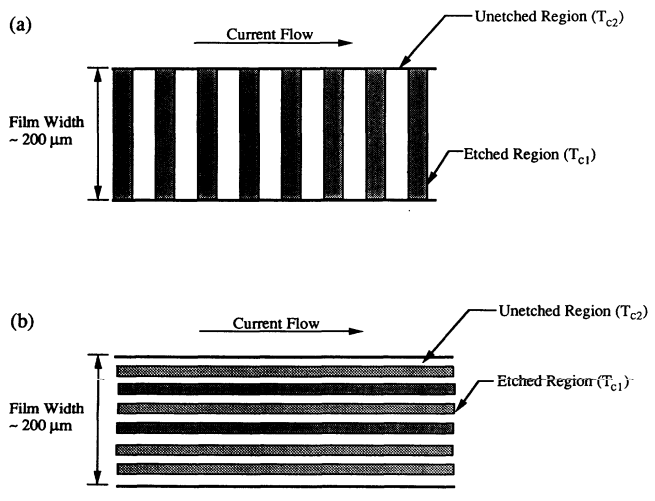

FIG. 1. Schematics of modulated-T_c structures, illustrating etched and unetched regions whose transition temperatures are T_{c1} and T_{c2}, respectively. We refer to the modulation in (a) as perpendicular while that in (b) as parallel.

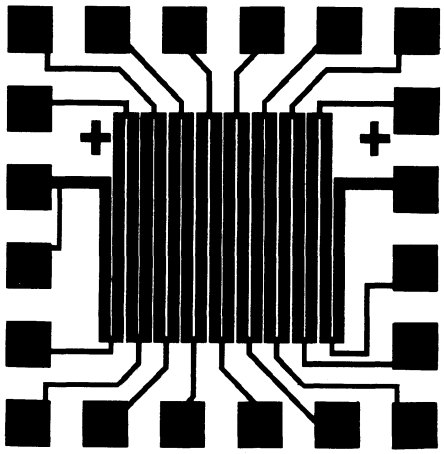

FIG. 2. Layout of a typical sample. This structure contains 14 modulated films together with the uniformly etched and uniformly unetched films electrically in series. Each film constitutes a leg of this meander pattern. The associated leads and square bonding pads permit individual films to be connected to a four-terminal resistance bridge.

The CHF_3-O_2 plasma employed is typically used for etching Si_3N_4. As such, exposing the aluminum film to such a plasma is not formally an etch, and no appreciable amount of aluminum is expected to be removed as a result. For convenience, we will continue to refer to the region of the film exposed to the plasma as the etched region.

Due to the excellent etch resistance of photoresist, the edge roughness of the resulting etched-unetched interfaces is expected to be better than $\pm 0.2\,\mu$m, the typical line width control of our photolithographic process. Using scanning electron microscopy and Auger electron microanalysis, we have ascertained that this process, indeed, gives rise to sharp interfaces on a length scale better than 1 μm. Further, by Auger depth profiling, we found that only surface damage results in the etched region.

The plasma apparently interacts only with the native oxide residing on the top 50 Å of the aluminum film. This oxide surface layer is always present upon exposure of the film to room air. Auger electron analysis indicates that within this top surface layer, oxygen content is reduced while the fluorine content is enhanced in the etched regions. This is clearly seen in the Auger line scans of Fig. 3. Here, the fluorine and oxygen signals are plotted as a function of position along a film with $d_1=d_2=10\,\mu$m. Although the magnitude and the sign of ΔT_c is fairly sensitive to the exact process conditions, the depression of T_c in the etched region is clearly correlated with a suppression of oxygen, which is consistent with the behavior for aluminum reported in the literature.

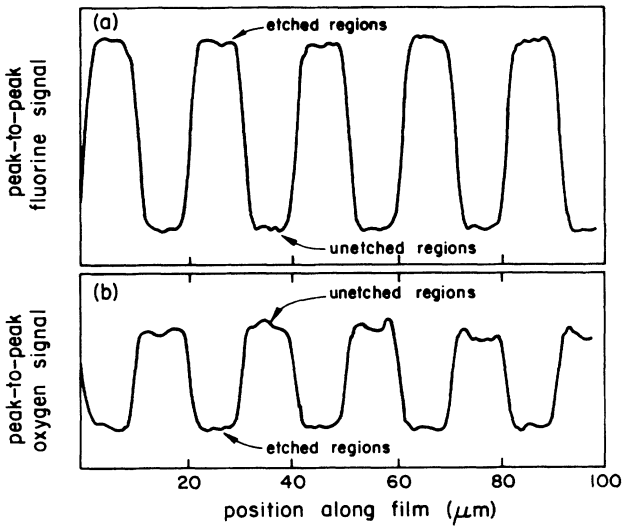

FIG. 3. Line scans of Auger signals. Auger peak signals for fluorine (a) and oxygen (b) are shown across several etched and unetched regions of a modulated film. The spatial resolution of these scans is limited by the size of the electron beam in the analytical instrument, which is somewhat better than 2 μm. Images obtained from scanning electron microscopy indicate that interface sharpness is better than 1 μm.

The role of the fluorine is as yet unclear, aside from its apparent propensity for replacing oxygen.

Besides the suppression of the T_c by a few percent, the etching process is noninvasive to the film's other transport properties. First, the normal-state transport properties are not substantially degraded. The resistance rises by $<20\%$, the residual resistance ratio (RRR) decreases by $<0.5\%$, and the low-temperature value of D decreases by $<10\%$. More importantly, the width of the resistive transition (which we define as the temperature range for which the resistance drops from 90% to 10% of its normal-state resistance) is about the same before and after etching, both ~ 10 mK. Lastly, as determined from quantum transport studies, the inelastic-scattering rate is not substantially increased by the etch.

We have carried out magnetoresistance measurements[12,13] on etched films together with contiguous unetched films. These measurements were performed in the normal state for $H<300$ G and $1.5<T<7$ K. By fitting these data to the theories of weak localization and superconducting fluctuations, we can obtain the inelastic-scattering (dephasing) rate, $\tau_{\rm in}^{-1}$, as a function of temperature. For typical etching times used, we have established that both the etched and unetched films exhibit nearly identical values of $\tau_{\rm in}^{-1}$. Also, the same temperature dependence of this rate, $\tau_{\rm in}^{-1}\sim AT+BT^3$, was observed for temperatures up to ~ 7 K. These results further confirm the noninvasive nature of our process and are useful for later discussions.

III. EXPERIMENTAL RESULTS

In order to investigate the resistive transitions of these structures, we have patterned the films in four basic configurations: (i) perpendicular modulation [see Fig. 1(a)] with d_1/d_2 held fixed and the modulation period, $\Lambda=d_1+d_2$, varied; (ii) perpendicular modulation with d_1, or d_2, held fixed and the ratio d_1/d_2 varied; (iii) same as (ii) except the modulation is parallel [see Fig. 1(b)], rather than perpendicular, to current path; and (iv) quasiperiodic perpendicular modulation. As the exact T_c's tend to vary somewhat from sample to sample, we have found it convenient to study samples containing a multiple number of these configurations (usually two), thus allowing a systematic examination of the T_c of the modulated structures for particular values of T_{c1} and T_{c2}.

We have made measurements on a total of 11 samples, denoted by an upper-case letter. Each sample typically consists of two data sets with different configurations of d_1 and d_2, referred to as data sets "0" and "1." (Thus, the two data sets on sample F are "$F0$" and "$F1$," respectively.) Unless otherwise specified, all measurements were carried out at a current density of 6 A/cm^2, using a standard four-terminal ac resistance bridge operating at 17 Hz. Each measurement is averaged over a minimum of 30 readings.

Thermometry is achieved by monitoring the resistance of a calibrated germanium sensor. For structures with a single sharp resistive transition, T_c is well defined. For these structures, we have chosen the T_c as the temperature where the normalized resistance equals one-half. Since the widths of the resistive transitions are similar for all films with single sharp transitions, a different criterion for T_c would not affect the conclusions of this paper. The uncertainty in T_c is taken to be ± 0.5 mK, the stability of our temperature control during a ramp.

A. Existence of a long length scale

The striking nature of the resistive transitions is shown in Figs. 4(a) and 4(b) (data sets $F0$ and $D0$), in which the normalized resistance of the various films is plotted against the temperature. In these samples, the ratio d_1/d_2 was maintained at unity, while Λ was varied from 4 to 400 μm. In Fig. 4(a), we plot the normalized resis-

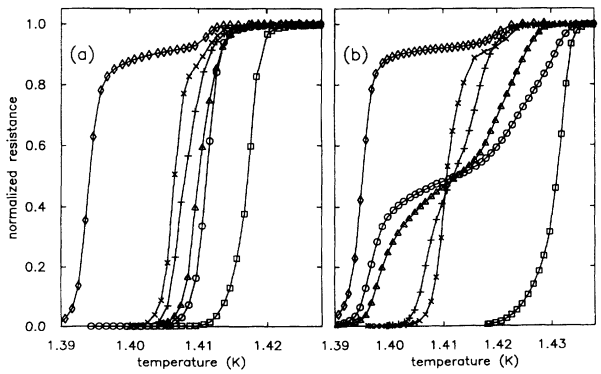

FIG. 4. Resistive transitions with unity ratio d_1/d_2 for data sets $F0$ (a) and $D0$ (b). In both (a) and (b), $\Diamond$ and $\square$ are the uniformly etched and unetched films. In (a), resistive transitions shown are: $\times$, $+$, $\triangle$, and $\circ$ for $\Lambda=4$, 10, 20, and 100 μm. In (b), resistive transitions shown are: $\times$ $+$, $\triangle$, and $\circ$ corresponding to $\Lambda=20$, 100, 200, and 400 μm.

tance of four films with $\Lambda=4$, 10, 20, and 100 μm, along with the normalized resistance of a uniformly etched film on the left and a uniformly unetched film on the right. This sample exhibits sharp resistive transitions for modulation periods $\leq 100\,\mu$m. An increase in Λ produces an *increase* in T_c of the modulated structure, as observed in all samples measured in this study. Figure 2(b) illustrates the onset of discrete transitions in another sample for $\Lambda \geq 100\,\mu$m. A pronounced shoulder develops at the half-resistance point, consistent with the geometry. Taken together, these observations suggest the existence of a long length scale over which superconductivity persists.

A number of systematic features should be discussed. The shoulder observed at a normalized resistance of ~ 0.9 is an artifact of sample geometry and is caused by *S-N* interfaces between leads and the structures under study. It should be emphasized that this feature is present even in the uniformly etched film and is unrelated to the onset of the resistive transition in the modulated structures. It can be eliminated if the leads and bondings pads are uniformly etched. As expected, the resistive transitions are sensitive to ΔT_c. This has the effect of shifting the onset of discrete transitions to larger Λ for samples with smaller ΔT_c.

Previous experiments have propagated supercurrent across dirty *S-N-S* junctions of many coherence lengths. To assess the strength of the proximity effect in our system, we have measured the effect of higher excitation currents and weak applied magnetic field. In Fig. 5, we plot again the resistive transitions for the etched, unetched, and the $\Lambda=100$ μm films of Fig. 4(a). The suppression of the temperature of the resistive transition is shown for the etched and $\Lambda=100$ μm films at current densities up to 600 A/cm^2. The sharp and uniform nature of the transitions are maintained at these current densities. (Higher current densities could not be explored using these samples due to heating effects.) For homogeneous thin films close to T_c, the current density varies as[10] $J_c=J_{c0}(1-T/T_c)^{3/2}$. For the uniformly etched film, we estimate (using the data of Fig. 5) the constant J_{c0} to be $\sim 2.3\times 10^6$ A/cm^2, which is a reasonable value for thin films.

A magnetic field of 1 mT produced noticeably broader transitions and suppressed T_c by ~ 50 mK. However, the homogeneous signature of the resistive transition was preserved in these fields. Typical thin-film behavior was observed down to ~ 0.4 K, in fields up to 30 mT.

B. Monotonic dependence of T_c on d_1/d_2

We now focus on the regime when $d_1 < 50\,\mu$m. In this limit, the modulated films exhibit a single sharp resistive transition with a well-defined T_c. In Fig. 6, we plot the resistive transition of a sample with $\Delta T_c=35$ mK. For this sample, d_1 is fixed at 5 μm, while d_2 is varied from 1 to 20 μm. As expected, the T_c's of these modulated films are between T_{c1} and T_{c2}, the T_c's of the uniformly etched and unetched controls. The transitions are shifted monotonically to a higher temperature as d_2 is increased.

Choosing the half-resistance temperature as the criterion for T_c, we can examine the dependence of T_c on d_1/d_2. For the sample of Fig. 6, the monotonic dependence of the T_c on this ratio is clearly illustrated as (○) in Fig. 7. In two other samples with $\Delta T_c \sim 25$ mK, d_1 was fixed at 5 μm in one, while d_2 was fixed at 5 μm in the other. In these samples, the dependence of T_c on d_1/d_2 is similarly monotonic. It is, in fact, identical within experimental scatter. This result is shown in the inset of Fig. 7.

The monotonic dependence of T_c on d_1/d_2 indicates that the samples produced by the etching technique are free from artifacts. First, although our technique induces surface damage only, the undamaged section beneath the surface of the film is not electrically shunting the top, which would have resulted in all the transitions having approximately the same T_c. This should be obvious considering the fact that the coherence length is substantially longer than the thickness of the film, and the system is,

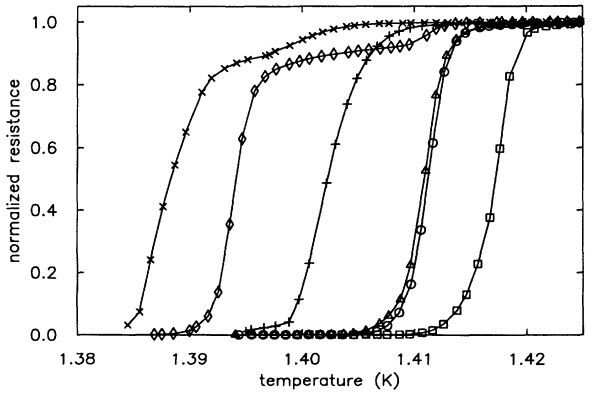

FIG. 5. Resistive transitions of uniformly etched (◇), unetched (□), and $\Lambda=100$ μm (○) films at a current density of 6 A/cm^2. Also shown are results at 60 A/cm^2 for the $\Lambda=100$ μm (△) film; and at 600 A/cm^2, the etched (×), and $\Lambda=100$ μm (+) films. Note homogeneous transitions for all current densities used, confirming the existence of a long length scale.

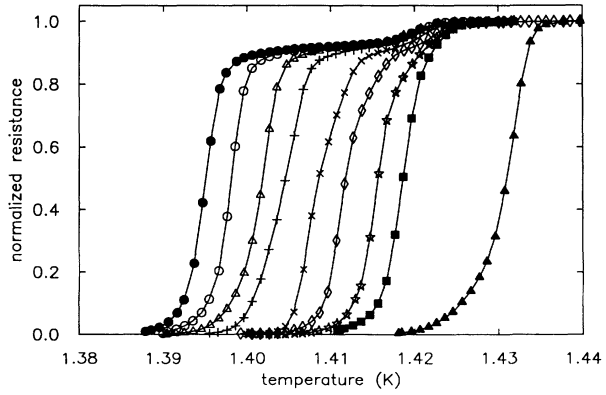

FIG. 6. Resistive transitions for data set *D*1, $\Delta T_c=35$ mK, in which the ratio of etched to unetched lengths (d_1/d_2) is varied from 0.2 to 5 while d_1 is fixed at 5 μm. ● and ▲ are the uniformly etched and uniformly unetched films, respectively. Symbols ○, △, +, ×, ◇, ☆, and ■ correspond to films with $d_2=1$, 2, 3, 5, 7, 10, and 20 μm, respectively.

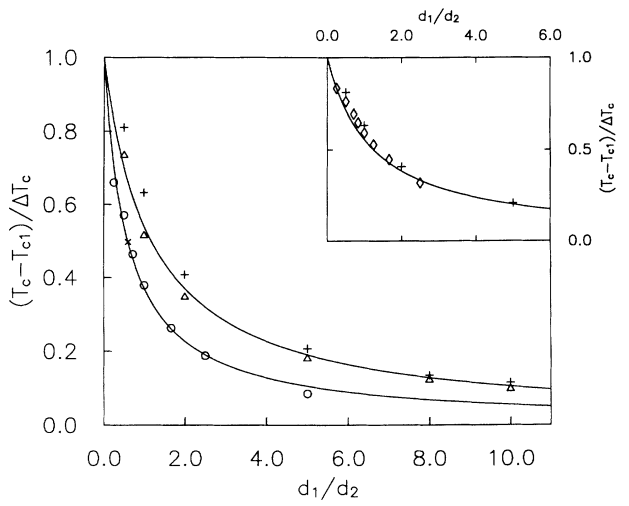

FIG. 7. Normalized T_c shift vs d_1/d_2 for various samples. Data set $D1$ of Fig. 6 is replotted here (○), illustrating the monotonic dependence of T_c on d_1/d_2. A Fibonacci lattice (×) on the same sample as $D1$ yields a T_c compatible with the periodically modulated films. (See Sec. III D.) Data sets $E0$ (△) and $E1$ (+) belong to a single sample with $\Delta T_c = 24$ mK, for which $d_2 = 2$ μm for $E0$ and $d_2 = 5$ μm for $E1$. Note that for a given value of ΔT_c, T_c depends primarily on the ratio d_1/d_2 and only weakly on their absolute magnitudes. In the inset, data set $E1$ (+) is replotted along with data set $C0$ (◇). $C0$ has $d_1 = 5$ μm and $\Delta T_c = 25$ mK. Note the same dependence of T_c on d_1/d_2 even though the etched length, rather than the unetched length, is fixed in $C0$. Solid lines are fits to Eq. (13) in the text.

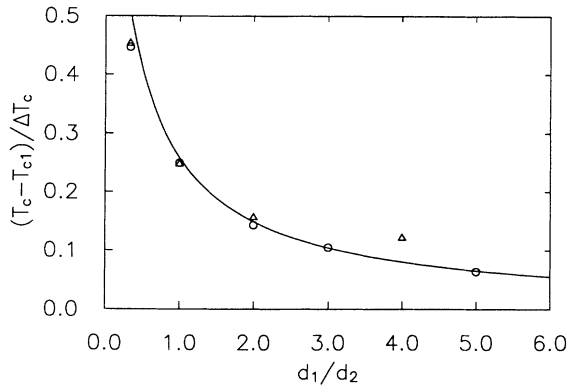

FIG. 8. Demonstration of the insensitivity to modulation direction. Here, the normalized T_c vs d_1/d_2 is plotted for data set $S0$ (○) with perpendicular modulation and data set $S1$ (△) with parallel modulation. This sample has $\Delta T_c = 50$ mK and $d_2 = 3$ μm. The solid line is a fit to Eq. (13) in the text. Uncertainty in the normalized T_c is approximately the size of the symbol. For a discussion of the uncertainty in d_1/d_2, see the text.

therefore, quasi-two-dimensional with respect to its superconducting properties. Second, the etching produces sharp S-N interfaces. If the interface were not sharp on the scale of ~1 μm, the monotonic dependence depicted in Fig. 7 would be absent. Further, we would have expected substantial differences in the behavior of the two samples plotted in the inset of Fig. 7. (The sharpness of the interface was also independently verified by microcharacterization techniques and scanning electron microscopy, as discussed above.) Consequently, we conclude that the long-range proximity effect is not an artifact of the processing.

For the proximity effect to exhibit a long range on the order of 50 μm, the T_c of the modulated structures should *not* depend sensitively on the absolute magnitudes of d_1 and d_2 when $d_1, d_2 < 50\,\mu$m. This is, indeed, observed. In Fig. 7 (+ and △), we show data from a single sample containing films for which d_2 is fixed at 2 or 5 μm, respectively. We note that the dependence of T_c on d_1/d_2 is approximately the same for both values of d_2. There is a slight systematic shift to higher T_c for the $d_2 = 5\,\mu$m films, but this effect is small. We note that the shift upward of the T_c with increasing d_2 is consistent with the observation of Fig. 4(a), for which d_1 and d_2 were increased but d_1/d_2 was fixed at unity.

C. Independence from modulation direction

We have also examined the dependence of the T_c on the direction of the modulation. In Fig. 8, we plot two data sets for films on a single substrate with d_2 fixed to be 3 μm. The direction of modulation is perpendicular to current flow in one data set and parallel in another, as depicted in Figs. 1(a) and 1(b). We see that both modulation directions result in the same T_c as the ratio d_1/d_2 is varied. Note that the film width (fixed at 200 μm) is, in general, not an integral multiple of the modulation period Λ. Thus, the regions along the film edge, which are always etched, will be narrower than the designated value of d_1. For small values of d_1/d_2, the number of modulation periods across the film is large, and this effect is unimportant. However, this effect becomes important at larger values of d_1/d_2, consistent with the deviation between the two data sets in Fig. 8 at large d_1/d_2.

The independence on modulation direction means that the unetched region is not electrically shunting the etched region. Thus, the film as a whole exhibits a single-transition temperature. Also, for the current density used, our measurements are free from complication by self-heating or nonequilibrium effects associated with N-S interfaces.[14] Thus, the observed resistive transitions reflect transitions of the order parameter and give the thermodynamic T_c. Of course, these results are further evidence that the system is free from fabrication related artifacts.

D. Quasiperiodic modulation experiment

We have explored whether periodicity is an important aspect of this system. To do so, we have modulated the T_c of some of the measured films in a controlled aperiodic fashion, according to the Fibonacci series:

$$u, ue, ueu, ueuue, ueuueueu, \ldots .$$

Here, u and e denote 5-μm-long unetched and etched regions, respectively. The series is continued for a total length of 400 units to fill the 2-mm length of the film. By counting the total number of u and e, it can be verified that the total etched length to the total unetched length is ~0.6 for this structure. This quasiperiodic modulation

scheme has been previously applied[15] to study semiconductor heterostructures.

Figure 7 shows that the Fibonacci film (×) has a T_c which is compatible with the periodically modulated films prepared on the same substrate. This suggests that the periodicity of these structures is unimportant.

IV. COMPARISON WITH MODELS

A. Breakdown of the dGW description

The mean free path l of our aluminum films is ~120 Å, using $v_F = 1.3 \times 10^8$ cm/s and the experimentally obtained diffusion constant of 50 ±5 cm^2/s. This value of l is much less than the intrinsic coherence length for aluminum ($\hbar v_F / 2\pi k_B T_c \sim 1.3\,\mu$m). Thus, our system is dirty; a necessary condition for the dGW theory.

Within the dGW description, the order parameter (pair wave function) ψ decays exponentially in the N region with a characteristic length K_N^{-1} given implicitly[16] by the transcendental equation:

$$\ln\left[\frac{T}{T_{cN}}\right] = \Psi\left[\frac{1}{2}\right] - \Psi\left[\frac{1}{2} - \frac{\hbar D K_N^2}{4\pi k_B T}\right] . \quad (1)$$

Here, $T_{cN} \equiv T_{c1}$, D is the diffusion constant of the N region, and Ψ is the digamma function. For the $\Lambda = 100$ μm film of Fig. 4(a), $T_{cN} = 1.394$ K. With this value, the decay length K_N^{-1} can be calculated numerically for $T > T_{cN}$. The results for $T/T_{cN} \sim 1$ are plotted in Fig. 9. Note that for $T/T_{cN} > 1.01$, $K_N^{-1} < 1$ μm and that even for $T/T_{cN} = 1.0005$, $K_N^{-1} < 5$ μm. For the $\Lambda = 100$ μm film, the resistive transition occurs at a temperature of 1.412 K. This corresponds to $T/T_{cN} = 1.013$ and, thus, K_N^{-1} is expected to be less than 1 μm.

For convenience, Clarke[1] has used the following closed-form expression for K_N^{-1}:

$$K_N^{-1} = \xi_N(T)\left[1 + \frac{2}{\ln(T/T_{cN})}\right]^{1/2} , \quad (2)$$

in which the so-called normal coherence length $\xi_N(T) = (\hbar D / 2\pi k_B T)^{1/2}$ is ~650 Å. To within ±10%, the values of K_N^{-1} obtained from Eqs. (1) and (2) agree with each other for T/T_{cN} as small as 1.0005, as seen in Fig. 9. For comparison purposes only, the function $K_N^{-1} = \xi_N(T)(T/T_{cN} - 1)^{1/2}$ is also plotted in Fig. 9 (dashed line). This is the form of the Bardeen-Cooper-Schrieffer (BCS) coherence length close to T_c. Note that the divergence of K_N^{-1} in T/T_{cN} of the BCS form is somewhat slower than (1) and (2).

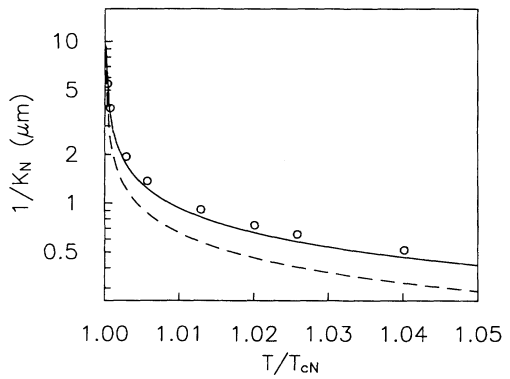

FIG. 9. Theoretical predictions of the order-parameter decay length K_N^{-1} as a function of reduced temperature close to T_{cN}, which is fixed at 1.394 K. The result of the transcendental equation (1) is evaluated numerically at a few temperatures (○). The solid line is the result of the approximate equation (2) of Clarke, which agrees well with Eq. (1). The dashed line is the BCS form $K_N^{-1} = \xi_N(T)(T/T_{cN} - 1)^{-1/2}$. Note that K_N^{-1} diverges slower in the BCS form than in Eqs. (1) and (2) as T/T_{cN} approaches 1. But, in all cases, $K_N^{-1} < 1\,\mu$m for $T/T_{cN} > 1.01$.

Previous experiments have propagated supercurrents across dirty *S-N-S* junctions of many coherence lengths.[1,6] The critical current density J_c of these junctions has been found to scale as $J_c = J_0(1 - T/T_{cS})^2 \exp(-K_N d_N)$, where $d_N \equiv d_1$. For parameters of the $\Lambda = 100$ μm film ($d_N = 50\,\mu$m) of Fig. 4(a), the exponential factor is of order 10^{-27}. The constant J_0 is typically less than 10^7 A/cm^2 in thin films, implying that J_c would be vanishingly small. This is clearly incompatible with our measured current density of *at least* 6 A/cm^2 close to T_c.

The dGW theory has been successful in describing experiments in the dirty limit to date. Our work concentrates on a system where the S and the N regions have nearly identical T_c's. This regime has not been previously explored experimentally. Provided that the gap parameters are small (always satisfied near T_c), there is no obvious reason to exclude the applicability of the theory to our system. As will be discussed further, it is likely that Josephson tunneling across a *S-N-S* barrier and the resulting single-exponential description of the order-parameter decay are not appropriate for our system. To elucidate the anomalous nature of this system, we now examine the data for films with $d_1 < 50\,\mu$m, which exhibit single sharp transitions. This is a regime suitable for a more detailed comparison with theories.

B. The single transition limit: The Ginzburg-Landau regime

Jin and Ketterson[17] have solved the problem of a two-component superlattice in the Ginzburg-Landau (GL) regime. In the limit $T \to T_c$, the order parameter ψ obeys the linearized GL equation. For spatial variation only in one direction without an applied field, the equation is

$$\frac{\hbar^2}{4m}\frac{d^2\psi}{dx^2} = a(T)\psi . \quad (3)$$

The coefficient $a(T)$ is related to the GL coherence length ξ via

$$a(T) = -\frac{\hbar^2}{4m\xi^2} = \alpha(T_c - T) , \quad (4)$$

where α is a temperature-independent factor and m is the effective mass of the carriers. Note that our modulated structures satisfy the GL limit because $T_{c1} < T < T_{c2}$ and $T_{c2}/T_{c1} \sim 1.04$.

Equation (3) holds separately in the etched regions and the unetched regions. Defining a common coordinate system (where $0<x<d_1$ is the etched region with $T_c=T_{c1}$ and $d_1<x<d_2$ is the unetched region with $T_c=T_{c2}$) and observing that the order parameters for the two regions, ψ_1 and ψ_2, must be symmetric with respect to the center of each region, we can write

$$\psi_1=A\cos\left[\frac{x-d_1/2}{\xi_1}\right], \tag{5}$$

$$\psi_2=B\cos\left[\frac{x-d_1-d_2/2}{\xi_2}\right]. \tag{6}$$

The appropriate boundary condition is that the logarithmic derivative at $x=d_1$ is continuous, i.e.,

$$p\frac{d}{dx}(\ln\psi_1)=\frac{d}{dx}(\ln\psi_2). \tag{7}$$

Here, p is a factor of order unity characterizing interface conditions.

The highest temperature for which a solution exists is identified as the T_c of the periodic structure. Applying the boundary condition (7) to (5) and (6) yields, for $T_{c1}<T<T_{c2}$,

$$\frac{p}{\xi_1}\tanh\left[\frac{d_1}{2\xi_1}\right]=-\frac{1}{\xi_2}\tan\left[\frac{d_2}{2\xi_2}\right]. \tag{8}$$

We now assume that the effective coherence lengths of the two regions are much larger than the modulation length scales, i.e., $\xi_1\gg d_1$ and $\xi_2\gg d_2$. This assumption is used in view of the long characteristic range of the proximity effect and that the system is in the single-transition limit. Its validity will be further discussed later. Thus, (8) reduces to

$$\frac{pd_1}{\xi_1^2}\approx-\frac{d_2}{\xi_2^2}, \tag{9}$$

which, according to (4), can be rewritten as

$$pm_1\alpha_1d_1(T_{c1}-T)=-m_2\alpha_2d_2(T_{c2}-T). \tag{10}$$

Solving for T gives the T_c of the modulated-T_c structure,

$$T_c=\frac{pm_1\alpha_1d_1T_{c1}+m_2\alpha_2d_2T_{c2}}{pm_1\alpha_1d_1+m_2\alpha_2d_2}. \tag{11}$$

The two different regions of our film have nearly equal T_c and normal-state transport properties. Thus, the ratios m_1/m_2 and α_1/α_2 should be near unity. These ratios can be incorporated into the factor p, which will be used as a fitting parameter in the following analysis of data. The transition temperature is then

$$T_c=\frac{pd_1T_{c1}+d_2T_{c2}}{pd_1+d_2} \tag{12}$$

or

$$\frac{\Delta T_c}{T_c-T_{c1}}=1+p\frac{d_1}{d_2}. \tag{13}$$

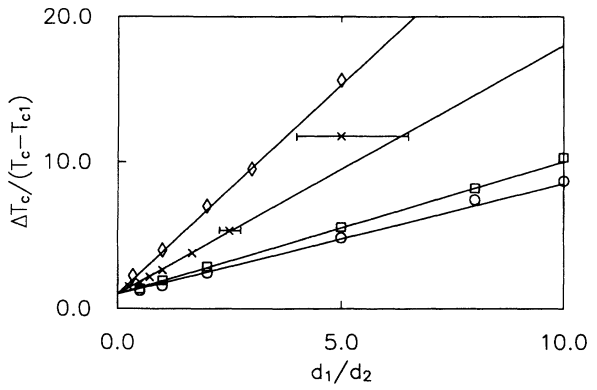

FIG. 10. Reduced data for data sets $E1$ (○), $E0$ (□), $D1$ (×), and $S1$ (◇), with $\Delta T_c=23.8$, 23.8, 36.0, and 50.0, respectively. The inverse normalized T_c shift is plotted against the ratio d_1/d_2. Solid lines are fits to Eq. (13) in the text for values of the parameter $p=0.75$, 0.9, 1.7, and 2.85, respectively. Error bars for $D1$ are due to systematic uncertainty in the fabrication feature size, typically $\pm0.2\,\mu$m.

Data for all samples studied fit surprisingly well to the simple expression (13), as evident in Fig. 10. The parameter p ranges from 0.75 to 2.85 for the four data sets plotted. For larger ΔT_c, p is shifted higher, but always of order unity. Deviation from the fit becomes pronounced for larger d_1/d_2 (not shown), corresponding to the eventual breakdown of the simple law at very long modulation length scales. In Figs. 7 and 8, the solid lines fitted to the data are, in fact, Eq. (13). However, since $(T_c-T_{c1})/\Delta T_c$ is plotted against d_1/d_2 in these graphs, the linear dependence of $\Delta T_c/(T_c-T_{c1})$ on d_1/d_2 is less apparent.

C. The Cooper–de Gennes limit

When $d_1,d_2\ll\xi_1,\xi_2$, the effective electron-electron interaction strength of a nonuniform system is a weighted average of the contribution of its constituents. In this limit, called the Cooper–de Gennes limit,[3]

$$NV=\frac{N_1^2V_1d_1+N_2^2V_2d_2}{N_1d_1+N_2d_2}. \tag{14}$$

Here, N is the density of states at the Fermi surface, V is the pair attraction potential, and the subscripts "1" and "2" again refer to the etched and the unetched sections, respectively. With NV specified, T_c is given by the usual BCS formula:

$$k_BT_c=1.14\hbar\omega_D\exp\left[-\frac{1}{NV}\right]. \tag{15}$$

Since T_c, T_{c1}, and T_{c2} differ by only a few percent, we can write

$$T_{c2}-T_{c1}=(N_2V_2-N_1V_1)\frac{dT_{c1}}{d(N_1V_1)}, \tag{16}$$

$$T_c-T_{c1}=(NV-N_1V_1)\frac{dT_{c1}}{d(N_1V_1)}. \tag{17}$$

Combining with Eq. (14), an expression similar to the GL

result, Eq. (13), is readily obtained:

$$\frac{\Delta T_c}{T_c - T_{c1}} = \frac{N_2 V_2 - N_1 V_1}{NV - N_1 V_1} = 1 + \frac{N_1}{N_2}\frac{d_1}{d_2} . \tag{18}$$

The ratio N_1/N_2 should be very close to unity in our system. Comparing with Eq. (13), we see that p should, indeed, be of order unity. Note that no explicit account of boundary effects is included, which is equivalent to taking $p=1$ in the GL analysis. The Cooper–de Gennes limit does not assume any inherent periodicity of the superlattice. Only the relative sizes of d_1 and d_2 matter. This is consistent with our observation that quasiperiodic (Fibonacci) modulation of the films gives rise to T_c's which are compatible with periodic modulation.

Provided that the assumption $d_1, d_2 \ll \xi_1, \xi_2$ is correct, these results suggest that we have acquired an understanding of the data in the single-transition limit ($d_1 < 50$ μm). Yet, based on the estimates of Sec. IV A, this assumption cannot be true for our system. We believe the good fit may be fortuitous. To explore this, we now compare our data with the results of a microscopic calculation involving no adjustable parameters.

D. Self-consistent field technique

General treatments of multicomponent superconducting systems were given by de Gennes[3,18] and, separately, by Takahashi and Tachiki[19] using the self-consistent-field (SCF) method of Bogoliubov. These techniques are applicable to general nonuniform systems. The relevant equations include the Bogoliubov equations and the self-consistency equations of the single-electron potential and the pair potential, both of which may vary in space. The superlattice in question is characterized by the periodic variation of the potentials in one direction and the appropriate boundary conditions at interfaces separating regions of different T_c's. Agreement between experiments and these calculations has been previously demonstrated. In particular, upper-critical-field measurements[20] showed good agreements with the predictions of Takahashi and Tachiki.

For a two-component superlattice composed of similar materials, Jin and Ketterson showed that these complex equations reduce to a particularly simple form. This result assumes that D, the density of states N, and the Debye frequency ω_D are constant, while the pair attraction potential V is the only varying microscopic parameter in the different regions of the system. This special case is remarkably similar to our modulated-T_c structures, and the result can be used directly without modification. The following paragraph states the relevant result in a form suitable for numerically evaluating the T_c of our modulated structures. Details of the derivation can be found in the review article by Jin and Ketterson.[17]

The transition temperature is identified as the highest temperature T for which a solution exists for the secular equation

$$\left| \delta_{mn} - \frac{2\pi}{\hbar} k_B T \sum_{\omega} \frac{\langle m|NV|n\rangle}{2|\omega| + \Omega_m} \right| = 0 , \tag{19}$$

where the outer vertical bars denote a matrix determinant. In our special case, the eigenvalues Ω_m are

$$\Omega_m = D\left[\frac{2\pi m}{d_1 + d_2}\right]^2 . \tag{20}$$

It can be shown that the summation over ω in (19) is given by

$$\frac{2\pi}{\hbar} k_B T \sum_{\omega} \frac{\langle m|NV|n\rangle}{2|\omega| + \Omega_m} = \langle m|NV|n\rangle \left[\ln\left[\frac{1.14\hbar\omega_D}{k_B T}\right] - \chi\left[\frac{\hbar\Omega_m}{2\pi k_B T}\right] \right] . \tag{21}$$

In (21), the function χ is defined as

$$\chi(x) = \Psi\left[\frac{x}{2} + \frac{1}{2}\right] - \Psi\left[\frac{1}{2}\right] , \tag{22}$$

where Ψ is the digamma function. In (19) and (21), the matrix elements are given by

$$\langle m|NV|n\rangle = \begin{cases} \dfrac{N}{\pi}(V_1 - V_2)\left[\dfrac{1}{m-n}\sin\left[\dfrac{\pi(m-n)d_1}{d_1+d_2}\right] + \dfrac{1}{m+n}\sin\left[\dfrac{\pi(m+n)d_1}{d_1+d_2}\right]\right], & m \neq n \\ \dfrac{N}{d_1+d_2}(V_1 d_1 + V_2 d_2) + \dfrac{N}{2\pi n}(V_1 - V_2)\sin\left[\dfrac{2\pi n d_1}{d_1+d_2}\right], & m = n \end{cases} . \tag{23}$$

Using the experimental values of T_{c1} and T_{c2}, the BCS equation (15) can be used to evaluate NV_1 and NV_2. With these values, $\langle m|NV|n\rangle$ can be calculated using (21) for $m, n = 1-10$. (Larger matrices do not give substantially different results.) Using (20) and (21), the $m \times n$ entries of the matrix in Eq. (19) can then be evaluated. To obtain the T_c of the modulated structure, values of T satisfying (19) are sought starting at T_{c2}, typically in decreasing order. The maximum T satisfying (19) is identified as the T_c of the system. Note that this pro-

cedure calls for no adjustable parameters aside from the experimental values of T_{c1} and T_{c2}.

Figure 11 shows the results of these calculations. In Fig. 11(a), we plot $\Delta T_c/(T_{c1}-T_c)$ vs d_1/d_2 for a sample with $d_2=2$ μm. As was shown in Fig. 10, Eq. (13) fits the data well with $p=0.9$. For comparison, the result of the Cooper–de Gennes limit ($p=1.0$) is also shown (dashed line), and the result of the SCF calculation is illustrated by the lower solid lines. Note that solution to (19) exists only for $d_1/d_2<2$, corresponding to a maximum permissible d_1 of ~ 4 μm. When d_2 is fixed at a smaller value, the range of d_1/d_2 over which solutions exists for (19) increases. However, the maximum d_1 for which such solution exists remains at ~ 4 μm. This is seen in Figs. 11(b) and 11(c), where $d_2=1$ and 0.5 μm, respectively. We interpret this as the maximum values of d_1 for which a single homogeneous transition should be observed in the modulated structures, consistent with the earlier theoretical considerations of dGW. Finally, in the limit that the modulation length scale is small ($d_2=0.1$ μm), the predictions of all three models approach each other, as seen in Fig. 11(d). This is expected since all three theories should be applicable in the limit that the modulation length scales are small in comparison with the coherence length. Since this length is ~ 1 μm according to the estimates of Sec. IV A, the different theories should yield the same results when d_1 and d_2 are simultaneously much less than 1 μm.

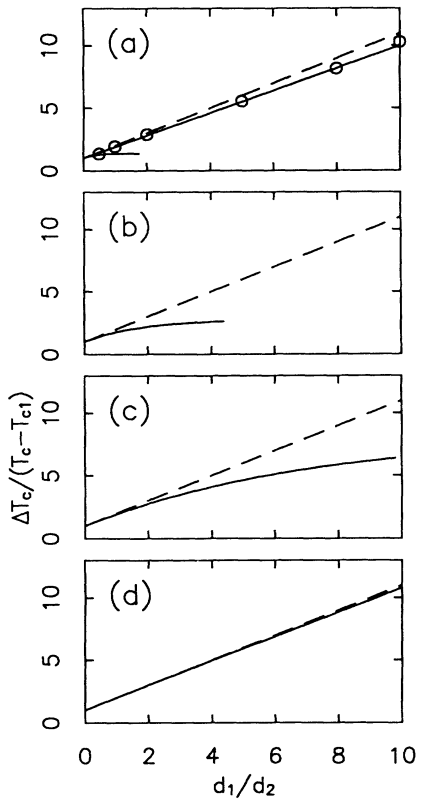

FIG. 11. Comparison of the results of the various theoretical models in the single-transition limit when $\Delta T_c=24$ mK. The four graphs correspond to $d_2=2\mu$m (a), 1 μm (b), 0.5 μm (c), and 0.1 μm (d). Actual data (○) are available for $d_2=2\mu$m (data set *E*0), which is fitted to Eq. (13) with $p=0.9$. The dashed line is the result of the de Gennes–Copper limit, Eq. (18). The lower curved solid line is the result of the self-consistent-field calculation, which yields no solution for d_1 above $\sim 4\mu$m, consistent with the dGW theory. As expected, in the limit that $d_1 \ll 1$ μm (d), all models converge to approximately the same result.

V. DISCUSSION

Our modulated-T_c structures exhibit an anomalously long-range proximity effect which is inconsistent with the accepted microscopic description of de Gennes and Werthamer. This long length scale persists even at very high current densities, suggesting that it is not the result of a vanishingly weak order parameter in the *N* region due to pair tunneling.

In the single-transition limit, the T_c of the structures depends monotonically on the ratio d_1/d_2, and rather insensitively on the absolute magnitudes of d_1 and d_2. These observations are consistent with the existence of a long-range proximity effect. We have also demonstrated that the modulation direction, as well as the periodic nature of the modulation, are unimportant, indicating that our interpretation is not complicated by artifacts. These results can be fitted to a phenomenological Ginzburg-Landau model and the result in the Cooper–de Gennes limit, which are applicable, *provided* that the modulation length scales d_1 and d_2 are much smaller than the coherence lengths in the two regions. Such an assumption is, however, incompatible with the estimated coherence length of our dirty aluminum film. Consistent with this statement is the failure of a microscopic SCF theory to fit the experimental results. Indeed, failure to fit data is an understatement since no solution exists at all within this theory for modulation lengths >4 μm. Therefore, according to this theory, the system should not exhibit a single transition when the *N* region exceeds this length.

We have suggested earlier that the single exponential decay description of the order parameter may simply be inadequate. However, there is no obvious reason why our system should be outside the regime of validity[1] for the dGW theory. We believe the failure of theories is linked in no small part to the similar T_c's of the *S* and *N* regions. (This is, after all, a previously unexplored regime.) Near T_c, the phase coherence of the quasiparticles can be maintained over long distances in aluminum.[21] For our films, we have determined, from quantum transport measurements, that the dephasing length close to T_c is on the order of a few μm.[12] It is possible that pairs enter a *N* region, break up, but traverse the *N* region without complete loss of phase memory. Once these quasiparticles reenter a *S* region, they readily recombine to form pairs. As such, the mechanism responsible for this long-range proximity effect may not be pair tunneling, but is, instead, connected with superconducting fluctuations.[22] Exactly how the quasiparticle coherence enhances the order parameter of the overall system awaits a detailed theoretical analysis.

In future experiments, it may be useful to systematical-

ly increase ΔT_c in a controlled fashion. The observation of a changeover from our long-range proximity effect regime to the conventional tunneling regime may be the key in understanding the present system. A large shift of the T_c cannot be easily achieved using the present etching technique. Alternative approaches might include decreasing the thickness of the aluminum films, using magnetic overlayers, or applying stronger etches to damage or remove the aluminium. In addition, a different material besides aluminum should be studied. However, significant change in the transport properties of the film as a result of a more invasive processing steps is to be expected. This will substantially increase the complexity of comparing data with theories. Recall that great simplifications in the three theories examined are possible precisely because $T_{c1} \sim T_{c2}$ and parameters such as D, N, m, α, and ω_D are roughly the same throughout the system.

In conclusion, we have carried out a survey of the properties of a 2D analog of a modulated transition temperature superlattice. The results are inconsistent with accepted theoretical models. It is possible that quasiparticle phase coherence plays an important role in understanding these results.

ACKNOWLEDGMENTS

We acknowledge helpful conversations with Professor R. Buhrman, Professor M. Tinkham, Professor V. Ambegaokar, Professor R. Silsbee, Professor D. Rainer, and Professor D. Prober during the various stages of this work. This research was supported by AFOSR 90-0111, the NSF through Grant No. DMR-90-16301, and the Cornell Materials Science Center under Grant No. DMR-88-18558. All fabrication work was performed at the Cornell National Nanofabrication Facility under the support of NSF Grant ECS 8619094. For the initial part of the research, Y.K.K. was supported in part by Tektronix, Inc., and K.L. was supported in part by IBM.

*Present address: Electronics Research Laboratory, Tektronix, Inc., Beaverton, OR.

†Present address: Department of Physics, SUNY, Stony Brook, NY.

[1]Clarke, Proc. R. Soc. London, Ser. A **308**, 447 (1969).

[2]G. Deutscher and P. G. de Gennes, in *Superconductivity,* edited by R. D. Parks (Marcel Dekker, New York, 1969).

[3]P. G. de Gennes, *Superconductivity in Metals and Alloys* (Benjamin, New York, 1966).

[4]N. R. Werthamer, Phys. Rev. **132**, 2440 (1963).

[5]Y. Krahenbuhl and R. J. Watt-Tobin, J. Low Temp. Phys. **35**, 569 (1979).

[6]J. G. Shepherd, Proc. R. Soc. London, Ser. A **326**, 421 (1972).

[7]T. Y. Hsiang and D. K. Finnemore, Phys. Rev. B **22**, 154 (1980).

[8]K. Lin, Y. K. Kwong, M. S. Isaacson, and J. M. Parpia, Physica B **165**, 483 (1990).

[9]Y. K. Kwong, K. Lin, M. S. Isaacson, and J. M. Parpia, Phys. Rev. Lett. **65**, 2905 (1990).

[10]M. Tinkham, *Introduction to Superconductivity* (Krieger, Malabar, FL, 1980).

[11]K. Lin, Y. K. Kwong, M. Park, J. M. Parpia, and M. S. Isaacson, J. Vac. Sci. Technol. B **9**, 3511 (1991).

[12]Y. K. Kwong, K. Lin, P. Hakonen, M. S. Isaacson, and J. M. Parpia, J. Vac. Sci. Technol. B **7**, 2020 (1989).

[13]Y. K. Kwong, K. Lin, M. S. Isaacson, and J. M. Parpia, J. Low Temp. Phys. (to be published).

[14]J. Clarke, in *Nonequilibrium Superconductivity,* edited by D. N. Langenberg and A. I. Larkin (Elsevier, New York, 1986).

[15]R. Merlin, K. Bajema, Roy Clarke, F.-Y. Juang, and P. K. Bhattacharya, Phys. Rev. Lett. **55**, 1768 (1985).

[16]P. G. de Gennes and J. P. Hurault, Phys. Lett. **17**, 181 (1965).

[17]B. Y. Jin and J. B. Ketterson, Adv. Phys. **38**, 189 (1989).

[18]P. G. de Gennes, Rev. Mod. Phys. **36**, 225 (1964).

[19]S. Takahashi and M. Tachiki, Phys. Rev. B **33**, 4620 (1986).

[20]M. G. Karkut, V. Matijasevic, L. Antognazza, J. M. Triscone, N. Missert, and M. R. Beasley, Phys. Rev. Lett. **60**, 1751 (1988).

[21]P. Santhanam, S. Wind, and D. E. Prober, Phys. Rev. B **35**, 3188 (1987).

[22]J. M. Gordon and A. M. Goldman, Phys. Rev. B **34**, 1500 (1986), and references cited therein.

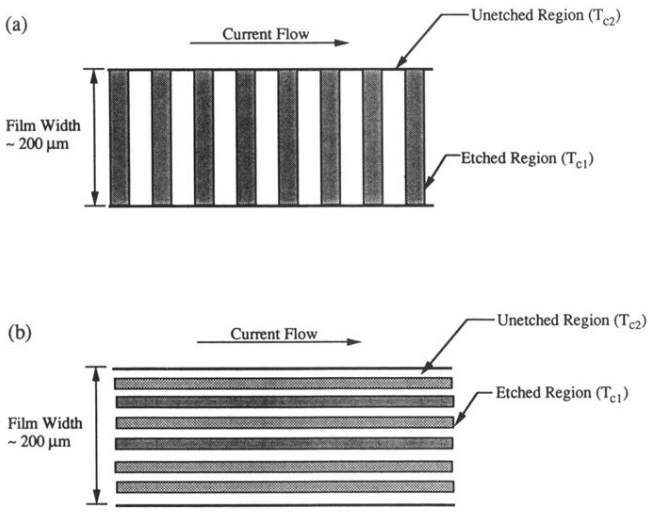

FIG. 1. Schematics of modulated-T_c structures, illustrating etched and unetched regions whose transition temperatures are T_{c1} and T_{c2}, respectively. We refer to the modulation in (a) as perpendicular while that in (b) as parallel.